



HAL
open science

Lithospheric structure of the central Andes based on surface wave dispersion

David Baumont, Anne Paul, George Zandt, Susan L Beck, Helle Pedersen

► **To cite this version:**

David Baumont, Anne Paul, George Zandt, Susan L Beck, Helle Pedersen. Lithospheric structure of the central Andes based on surface wave dispersion. *Journal of Geophysical Research: Solid Earth*, 2002, 107 (B12), pp.ESE 18-1-ESE 18-13. 10.1029/2001JB000345 . hal-02156825

HAL Id: hal-02156825

<https://hal.science/hal-02156825v1>

Submitted on 14 Jun 2019

HAL is a multi-disciplinary open access archive for the deposit and dissemination of scientific research documents, whether they are published or not. The documents may come from teaching and research institutions in France or abroad, or from public or private research centers.

L'archive ouverte pluridisciplinaire **HAL**, est destinée au dépôt et à la diffusion de documents scientifiques de niveau recherche, publiés ou non, émanant des établissements d'enseignement et de recherche français ou étrangers, des laboratoires publics ou privés.

Lithospheric structure of the central Andes based on surface wave dispersion

David Baumont^{1,2} and Anne Paul

Laboratoire de Géophysique Interne et Tectonophysique, Observatoire de Grenoble, Centre National de la Recherche Scientifique and Université Joseph Fourier, Grenoble, France

George Zandt and Susan L. Beck

Southern Arizona Seismological Observatory and Department of Geosciences, University of Arizona, Tucson, Arizona, USA

Helle Pedersen

Laboratoire de Géophysique Interne et Tectonophysique, Observatoire de Grenoble, Centre National de la Recherche Scientifique and Université Joseph Fourier, Grenoble, France

Received 11 February 2000; revised 31 December 2001; accepted 4 January 2002; published 26 December 2002.

[1] Shear wave velocity is very sensitive to temperature anomalies and partial melt and can provide important insights on the state of the lithosphere. With that aim in mind, phase velocities of Rayleigh and Love waves have been inverted for the regionalized shear wave velocity structure of the lithosphere across the central Andes. This inversion reveals strong lateral variations of V_s both across the range and along-strike in the Altiplano crust. In the upper crust, the main features of our models are prominent low-velocity anomalies probably related to partial melt below the Los Frailes ignimbrite complex and the southern Altiplano. At lower crustal level, the Altiplano is characterized by lower V_s than the surrounding regions. We find that the transition from the Altiplano to the Puna is associated with a 7-km thickening of the crust. At mantle depths, the Nazca plate is found to be overlaid by a dipping low-velocity zone with decreasing intensity with depth. Our results favor the idea of a cold mantle lid underlying the whole central Andes. **INDEX TERMS:** 7205 Seismology: Continental crust (1242); 7218 Seismology: Lithosphere and upper mantle; 7255 Seismology: Surface waves and free oscillations; **KEYWORDS:** Andes, surface waves, lithosphere, V_s , subduction

Citation: Baumont, D., A. Paul, G. Zandt, S. L. Beck, and H. Pedersen, Lithospheric structure of the central Andes based on surface wave dispersion, *J. Geophys. Res.*, 107(B12), 2371, doi:10.1029/2001JB000345, 2002.

1. Introduction

[2] The Andes are one of the largest active mountain ranges in the world, extending for over 8000 km along the western edge of the South American continent. In the central Andes major morphological changes occur in both the perpendicular and along-strike directions. North of 21°S, the mountain range is broad. From west to east, it includes the Western Cordillera (an active volcanic arc), the Altiplano (a wide, flat plateau), the Eastern Cordillera and the sub-Andean Range (fold and thrust belts). South of 21°S, in the Puna, the Andes narrow, reaching higher elevations (on average 1 km higher than in the Altiplano)

and a different tectonic style. These tremendous changes are not explained by simple mountain building processes. The mechanism behind the high elevation support of the central Andes is also unclear.

[3] In the last few years, geophysical investigations have provided a wealth of new data and models of the lithospheric structure [e.g., *Dorbath et al.*, 1993; *Wigger et al.*, 1994; *Dorbath et al.*, 1996; *Zandt et al.*, 1996; *Beck et al.*, 1996; *Myers et al.*, 1998; *Masson et al.*, 2000]. However, our knowledge of the upper mantle remains too sparse to understand its role in the mountain building processes. Indications of partial melt in the lower crust of the southern Altiplano found by *Wigger et al.* [1994], *Schmitz et al.* [1997], and *Schwartz et al.* [1994] were not confirmed by *Zandt et al.* [1996] and *Swenson et al.* [2000] in the central and northern Altiplano. As partial melt is a potential marker of tectonic shortening or magmatic intrusions of mantle origin in the crust, mapping the extension of related anomalies such as low-velocity zones (LVZ) is important to better understand the dynamics of the chain. A powerful tool for such analysis is the measurement of shear wave velocities, as they are very sensitive to temperature anomalies and partial melt. However, information on V_s are very

¹Also at Southern Arizona Seismological Observatory and Department of Geosciences, University of Arizona, Tucson, Arizona, USA.

²Now at Institut de Radioprotection et de Sûreté Nucléaire, Département de Protection de l'Environnement, Service d'Études et de Recherches sur la Géosphère et l'Élimination des déchets, Bureau d'Évaluation du Risque Sismique pour la Sûreté des Installations Nucléaires, Fontenay-Aux-Roses, France.

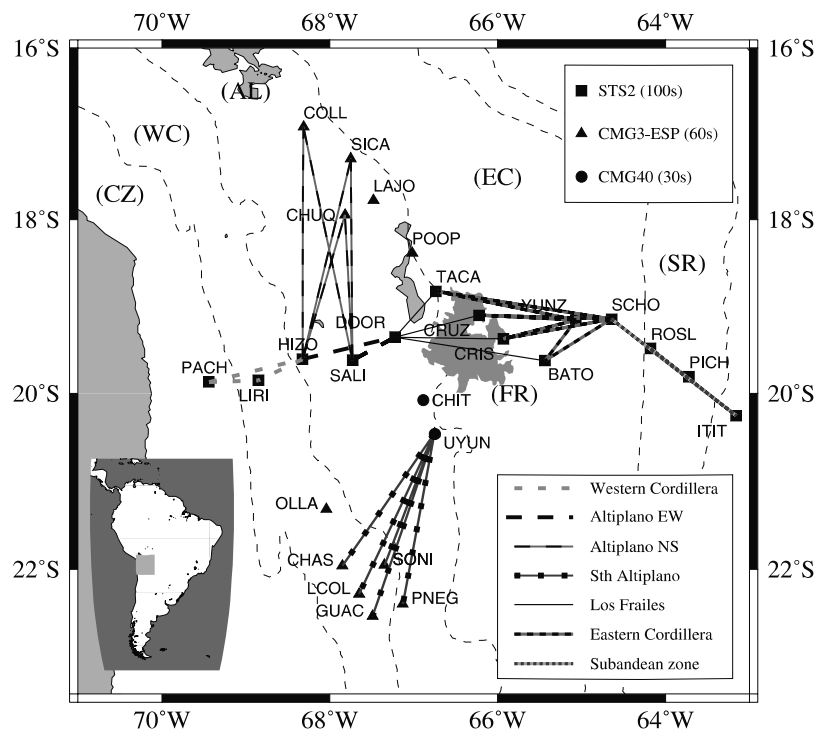


Figure 1. Map showing the station locations of the BANJO, SEDA, and southern Bolivian experiments and the paths along which we measured the interstation phase velocities. Paths corresponding to similar phase velocity dispersion curves are plotted using the same pattern. Note that each set of paths delineates a region corresponding to a single morphotectonic unit. These units are from west to east: Coastal Zone (CZ), Western Cordillera (WC), Altiplano (AL), Eastern Cordillera (EC), sub-Andean Range (SR), and Chaco Plain (CP). In the center of the figure, the outcrop of the Los Frailes (FR) volcanic complex is shaded.

scarce in this region [Myers *et al.*, 1998; Dorbath and Masson, 2000] and need to be complemented. Additional information can be obtained by inverting dispersion curves of surface waves for shear wave velocity structures which is also an efficient technique to probe the upper mantle. James [1971] first used this technique in the central Andes and proposed a V_s lithospheric model along a cross section located in the northern part of the Altiplano. Our purpose is to conduct a similar study at a higher resolution.

[4] In 1994, 1995, and 1996, three broadband seismic networks were deployed in the central Andes: the 18 month Broadband Andean Joint (BANJO) experiment, an east-west profile running across the main structural features of the chain, the 1 year Seismic Exploration of the Deep Altiplano (SEDA) experiment, a north-south profile located along the eastern boundary of the Altiplano, and an one year seismic network deployed in the southern part of the Altiplano and in the Altiplano-Puna Volcanic Complex. Figure 1 shows the station locations and the main tectonic units of the study area. Using teleseismic events recorded during these experiments, we determined the lateral variations of the shear wave velocity structure of the lithosphere, through the inversion of the regionalized phase velocity dispersion curves of the Rayleigh and Love waves.

2. Data Selection and Processing

[5] The methodology used here relies on the measurement of the phase variation between two stations for the funda-

mental mode of surface waves. This requires a reliable identification and extraction of the fundamental mode from the raw signal. This is simple for purely continental paths, fundamental modes of Rayleigh and Love waves are well separated from the higher modes in a group velocity versus period diagram as documented by computation of synthetic seismograms in a reference model like, e.g., PREM. The fundamental mode can therefore easily be identified and extracted from the raw signal. Whereas this still holds for Rayleigh waves propagating along a purely oceanic path, the identification of the fundamental mode is more difficult for the Love waves. In this case, several modes of the Love wave propagate with similar phase velocities and can therefore interfere with one another. Moreover, owing to the presence of low-velocity sediments on top of a typical oceanic crust, the amplitudes of the higher modes of Love wave can be larger than the fundamental for some double couples and in some particular directions as compared to the fault strike.

[6] In this study, most of the event-station paths include both continental and oceanic parts. This tends to separate the fundamental from the higher modes because their phase velocities are different along a significant part of the path. The propagation across the ocean-continent margin will also tend to partly redistribute the energy onto the fundamental mode further diminishing the problem of strong higher Love modes. However, to minimize any problems due to the presence of higher modes, we applied severe selection criteria to the data used in the measurement of the dispersion curves.

[7] To ensure a good signal-to-noise ratio, only events with a magnitude larger than 5.5 were used, except for the earthquakes located on the Mid-Atlantic Ridge where a magnitude 4.5 event generated signals with a good signal-to-noise ratio at our seismological stations. As the energy of higher modes usually increases with the earthquake depth, we selected teleseismic events located at depths smaller than 70 km in the U.S. Geological Survey National Earthquake Information Service (USGS NEIS) catalog (80% of the event depth are below 35 km). In addition, all data displaying a complex pattern in the time-frequency diagram [Dziwonski *et al.*, 1969; Herrmann, 1973; Levshin *et al.*, 1989] were rejected to avoid misinterpretation. The fundamental mode was identified by comparing the dispersion curves observed for all our source-station paths with typical dispersion curves of the fundamental modes for continental or oceanic paths [Oliver, 1962]. This analysis showed that no higher modes had significant energy with respect with the fundamental modes in our selected data set. The time-frequency analysis was also used to pick out possible problems in the data that might disturb the phase-velocity determination such as contamination by noise, spectral holes, or multipathing. Signals exhibiting multipathing were not used in this study because tests we made to measure interstation phase velocities using these signals (after extracting one particular branch of the dispersion curves) were not satisfactory as they showed large oscillations. Fundamental modes of the Rayleigh and Love waves were extracted by applying a phase-match filter [Levshin *et al.*, 1989] (see Figure 2) which significantly improves the phase-velocity determination. Each phase velocity measurement used in the inversion for a velocity-depth model results from the combination of measurements on several events located in very different source regions. This averaging limits the bias which would be introduced by a mixing of fundamental and higher modes. Finally, we inverted separately the Rayleigh dispersion curves and verified that the resulting V_s models were similar to the joint data inversion.

3. Phase Velocity Measurements

3.1. Methodology

[8] The ideal method for measuring the phase velocity between two stations is to select an earthquake with its epicenter located on the great circle joining the two stations and to divide the difference in travel time of a given phase by the interstation distance. The phase variation $\Delta\Phi$ of the wave train is evaluated using a Wiener filtering [Taylor and Toksoz, 1982] to minimize the influence of the residual noise, and the travel time difference is evaluated by $\Delta t = \frac{\Delta\Phi}{2\pi\nu}$, where ν is the frequency.

[9] In practice, the phase velocity determination is complicated by three main problems. First, for a detailed structural study like as this one, the interstation distance is smaller than the wavelength. No theoretical problem arises from that, but it is difficult to accurately measure very small phase variations. To improve our confidence in the phase velocity measurement, we cross-checked the results obtained using several events with different back-azimuths and epicentral distances and several station pairs to give a statistical estimate of the measurement uncertainty.

[10] The second problem is the counterpart of this statistical approach, as we must find several earthquakes with epicenters on the stations great circle which is practically impossible for data from temporary experiments. The only solution with a limited data set is to consider events located slightly away from the stations great circle. However, the rays that impinge on the two stations may then have sampled media with slightly different elastic properties resulting in an additional phase, so that the local geometry of the wave front might be affected. A third problem is that seismic rays are deflected from their great circle path by lateral variations of velocity [e.g., Laske and Masters, 1998; McGarr, 1969]. The ray deflection can reach an angle as large as 15° , as documented for instance by Laske *et al.* [1994] or Cotte *et al.* [2000]. In this case, the distance of propagation of the wave front between the two receivers, a function of the direction of arrival of the waves, is not correctly estimated leading to an incorrect evaluation of the phase velocity. The statistical approach partially addresses these last two problems by averaging the effect of the additional phase and ray deflection. However, a better solution is to perform a network analysis to deduce the orientation of the horizontal wave vector perpendicular to the wave front.

[11] Consequently, phase velocities were determined in four steps. For a given station pair, the first step consists in selecting the teleseismic events with the angle between the great circle propagation path and the interstation great circle smaller than 15° . This is necessary because the larger the angular offset, the larger the error made on the phase velocity when the back-azimuth is not correctly evaluated. For instance, for a 15° angular offset, a 5 to 10° error on the apparent back-azimuth determination results in a 2 to 7% change in phase velocity. As shown in Figure 3, very few measurements were made for a 15° great circle offset angle. For each region, the great circle offset angles we used are well distributed allowing us to evaluate the robustness of the measurements.

[12] The second step consists in measuring the actual orientation of the wave front for each event by performing a network analysis [Cotte *et al.*, 2000]. Considering the wave as plane within the network, for each frequency the travel time differences across the array were inverted to obtain the slowness vector, and thereby the propagation direction. However, solving reliably this problem requires to use stations deployed with a “triangle-like” geometry. To satisfy this condition given the geometry of the deployments, we used stations located slightly outside each study area, corresponding to network apertures of about 0.5 to 9 times the wavelength of the signal depending on the period. This whole processing was only applied to records with a signal-to-noise ratio larger than 5 and a correlation factor larger than 0.95. Figure 4 shows the observed ray deflection angle in the period range 30–35 s. For most events, this angle is smaller than 10° . In a few cases they are as large as 20° .

[13] The third step is the evaluation of the interstation phase velocities for each event using the observed back-azimuths, i.e., by calculating the velocities using the real distance covered by the wave train. In the final step, we calculate the mean of the phase velocity measurements and their standard deviation. In cases where the number of measurements is insufficient to give a correct statistical

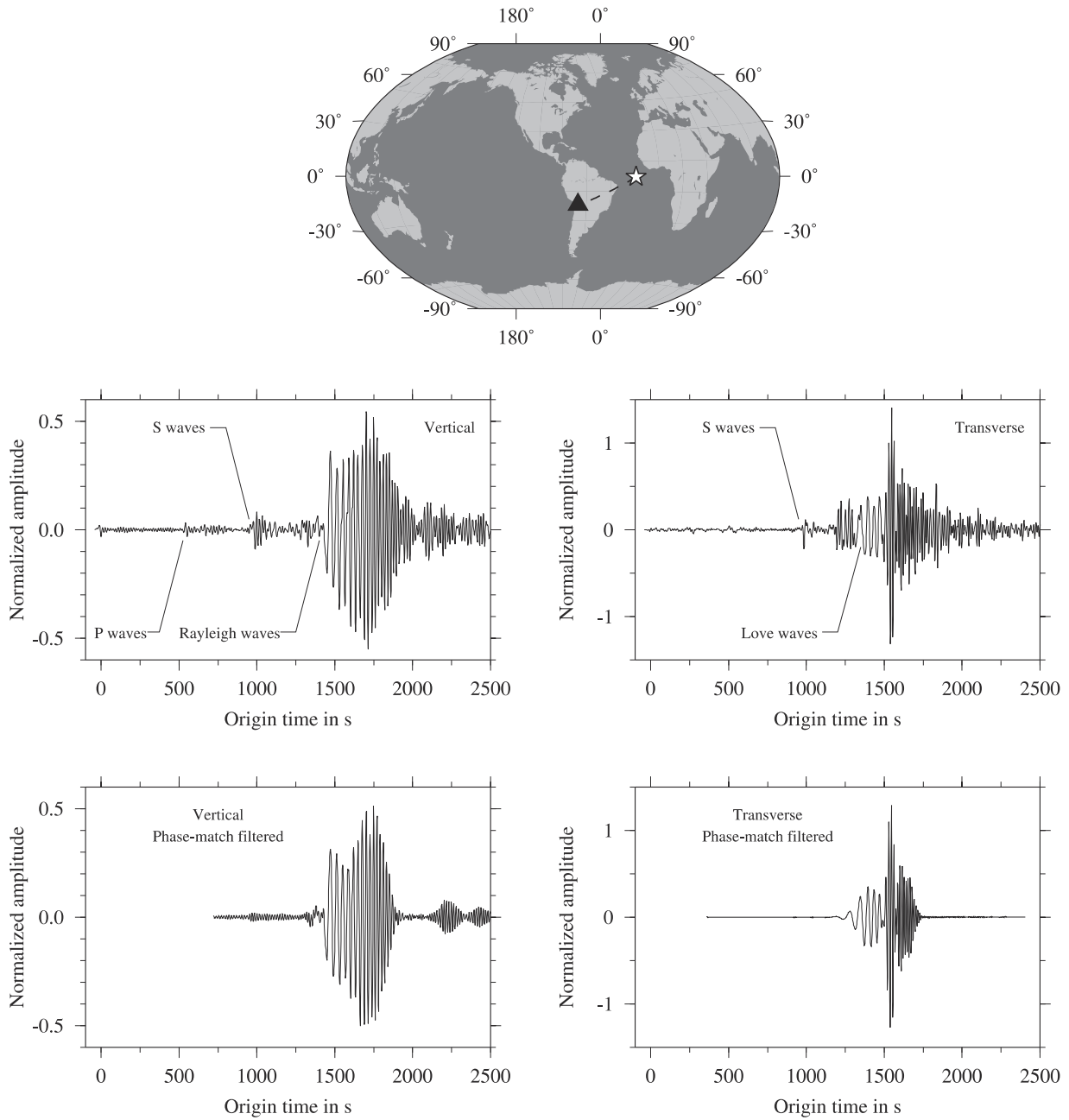


Figure 2. Example of the effect of phase-match filtering to extract the fundamental modes of Rayleigh and Love waves. Station and event locations are shown at the top of the figure. Vertical and transverse components of the record are shown before (middle) and after (bottom) phase-match filtering. Signals were deconvolved from the instrumental response of the sensor and filtered (vertical low-passed at 0.06 Hz and transverse band-passed between 0.01 and 0.08 Hz).

estimation, the envelope of dispersion curves is used to define a confidence domain.

3.2. Observations

[14] Because of the good station coverage (Figure 1), we were able to regionalize the phase velocity measurements so as to characterize the lithospheric structure accurately. This regionalization is based on the comparison of the phase velocity dispersion curves observed for all the station pairs. Interstation paths with similar velocity dispersion curves are shown in Figure 1. It shows that the regions defined from

the dispersion curve criterion correspond nicely to the morphotectonic units. Figure 5 displays the results of phase velocity measurements in each region. Note that we could not apply the network analysis to measure the back-azimuth deviation in the sub-Andes because the stations in this area were practically aligned in the direction of the source-station propagations along the very heterogeneous structures of the western coast of Americas (see locations of events in the inset of Figure 5g). However, we confirmed in the other regions that neglecting the ray deflection correction does not lead to erroneous results if the events are well

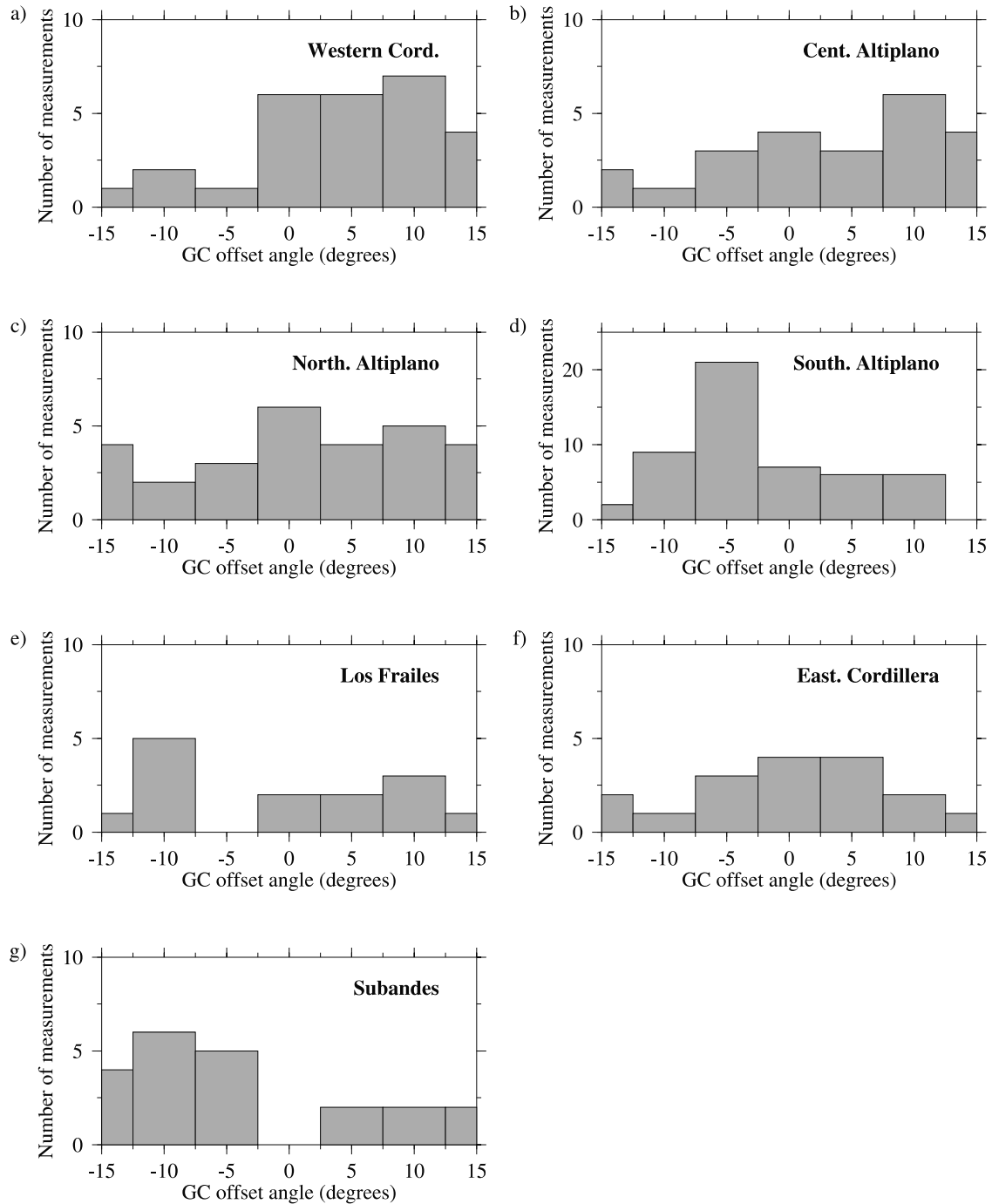


Figure 3. Histograms showing for each region the distribution of angular offsets between the great circle propagation path and the great circle connecting the station pairs used for the phase velocity measurements.

distributed in both epicentral distances and back-azimuths. As shown by Figures 3g and 5g, this condition is fulfilled in the sub-Andes.

[15] Figure 5 demonstrates that phase velocities vary strongly both across and to a lesser extent along the strike of the range. These lateral variations show that morphotectonic units are characterized by very different shear wave velocity structures. To easily compare our measurements, we also plotted in Figure 5 the Love and Rayleigh fundamental modes calculated for an Andean reference velocity

model. In the crust, this model is based on the results obtained by *Zandt et al.* [1996] for the Central Altiplano using forward modeling of intermediate depth earthquake waveforms recorded by BANJO and SEDA stations in the Altiplano. The mantle part of the reference model is derived from the velocities found by *James* [1971] for the northern Altiplano. Figure 5 proves that this model does not predict the dispersion curves measured in the Altiplano. In other words, actual crustal velocities are on average lower than in the Andean reference model.

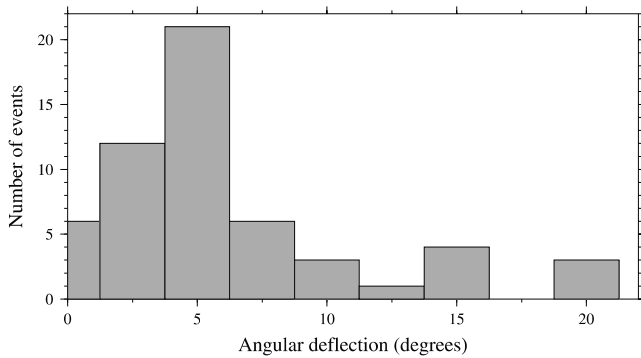


Figure 4. Histogram of seismic ray deflection angles measured from a network analysis on the observed travel time differences in the period range 30–35 s.

[16] As the lithosphere of the central Andes has been shown to be a highly attenuative medium for seismic waves [Wigger *et al.*, 1994; Ocola and Meyer, 1972; Myers *et al.*, 1998; Baumont *et al.*, 1999], and as anelasticity leads to dispersion [Azimi *et al.*, 1968; Liu *et al.*, 1976; Aki and Richards, 1980], one might conclude that dispersion curves are affected by attenuation. The quality factor is very poorly known in the frequency range of the surface waves. However, Figure 6 shows that for the minimum value of the intrinsic Q_s measured in the Altiplano at 1 Hz, i.e., $Q_s = 200$ [Myers *et al.*, 1998; Baumont *et al.*, 1999], the effect of anelasticity on the reference model dispersion curve is small in comparison with the margin of uncertainties of the measurements. Consequently, no corrections related to the anelasticity were applied on phase velocity measurements.

4. Inversion, Constraints, and Models

4.1. Methodology

[17] Observed dispersion curves were inverted for the average velocity structure using the two-step approach of Shapiro *et al.* [1997]. This technique explores a large model space and consequently makes it possible to estimate the uncertainty on the velocity structure. The first stage consists in a gradient inversion [Herrmann, 1987] of each average dispersion curve with an initial model based on previous geophysical investigations [Zandt *et al.*, 1996; Beck *et al.*, 1996; Myers *et al.*, 1998]. The number of layers was chosen to be as large as possible without leading to an ill-constrained inversion. The gradient inversion was performed for the S wave velocity in each layer and the depth of each interface. Density, Poisson's ratio and attenuation were held constant as the dispersion curves are only weakly sensitive to variations of these parameters.

[18] The second stage is an exploration of the model space to estimate the characteristics of all 1-D velocity models that satisfy the observations. Starting from the results of the gradient inversion, a set of models was generated by random perturbation of S wave velocities and interface depths. At each iteration, random model changes were bounded to 0.2 km s^{-1} for S wave velocities, and 20% for thicknesses. Phase velocities were then calculated for each model and compared to observations. If phase velocities predicted for a model were within the error bars of observations (Figure 5), then the model was retained and the

model space explored in its vicinity. More than 30,000 models were tested for a reliable sampling of the model space.

[19] In this study, to better constrain the inversion, the Love and Rayleigh dispersion curves were inverted simultaneously. However, as discussed in section 2.1, the Love waves may be somewhat influenced by interaction with higher modes. In addition, anisotropy would potentially yield different Earth models from Love and Rayleigh dispersion curves. We therefore also inverted the Rayleigh waves data alone and compared the results with the results from the joint Rayleigh and Love inversion. The comparison shows a slight tendency to attenuate the anomalies when Rayleigh wave dispersion curves are inverted alone, but the characteristics of the velocity models remain essentially the same. These very weak differences show that our joint inversions of Rayleigh and Loves wave dispersion curves are dominated neither by higher mode contamination, nor by anisotropy effects.

4.2. A Priori Constraints

[20] A priori constraints were added to the inversion to avoid unrealistic models. As they are presented for each region in Table 1, this section will only be devoted to the description of the main constraints. On the basis of several geophysical investigations conducted in the Altiplano [Beck *et al.*, 1996; Zandt *et al.*, 1996; Swenson *et al.*, 1999], we assumed a V_p -to- V_s ratio to be 1.73. Although lateral variations of V_p/V_s were documented in the central Andes by Dorbath and Masson [2000] and Myers *et al.* [1998], the weak sensitivity of the inversion to V_p justifies this choice.

[21] To model the presence of a sedimentary infill where it is well documented (i.e., in the northern and central Altiplano), V_s was limited to the range $2.3\text{--}3.2 \text{ km s}^{-1}$ in the first layer. Moreover, other crustal velocities were bounded by maximal values for a typical continental crust. Reasonable bounds on the crustal thickness were based upon previous geophysical results. In northern and central Bolivia, we relied on the receiver function analysis by Beck *et al.* [1996], the surface wave study by James [1971], and the interpretation of refraction data by Wigger *et al.* [1994]. In southern Bolivia, we used the results of the modeling of underside reflections for intermediate-depth earthquakes by Zandt *et al.* [1994]. Rather than assuming a 60–65 km crustal thickness beneath the central and northern Altiplano as computed by Beck *et al.* [1996] by estimating V_p/V_s but assuming V_p , we used their raw observation of Ps - P delay times. To that end, we selected the models which correctly predict these observations, (with a $\pm 3 \text{ km}$ tolerance on the crustal thickness). This constraint was only used in the northern and central Altiplano, as it is the only location where the average crustal V_p/V_s was measured accurately [Beck *et al.*, 1996].

[22] We also constrained the upper mantle S wave velocity to be between 4.4 and 4.75 km s^{-1} . These values are based on global upper mantle V_s observations [Gumper and Pomeroy, 1970; Huestis *et al.*, 1973; Ni and Barazangi, 1983; Brune and Dorman, 1963; Eaton, 1980] and include the range of values inferred in the local tomography of Myers *et al.* [1998]. We modeled the presence of the subducted slab by assuming its velocity to be between 4.8 and 5.1 km s^{-1} , corresponding to a V_s positive anomaly of 2–8% with

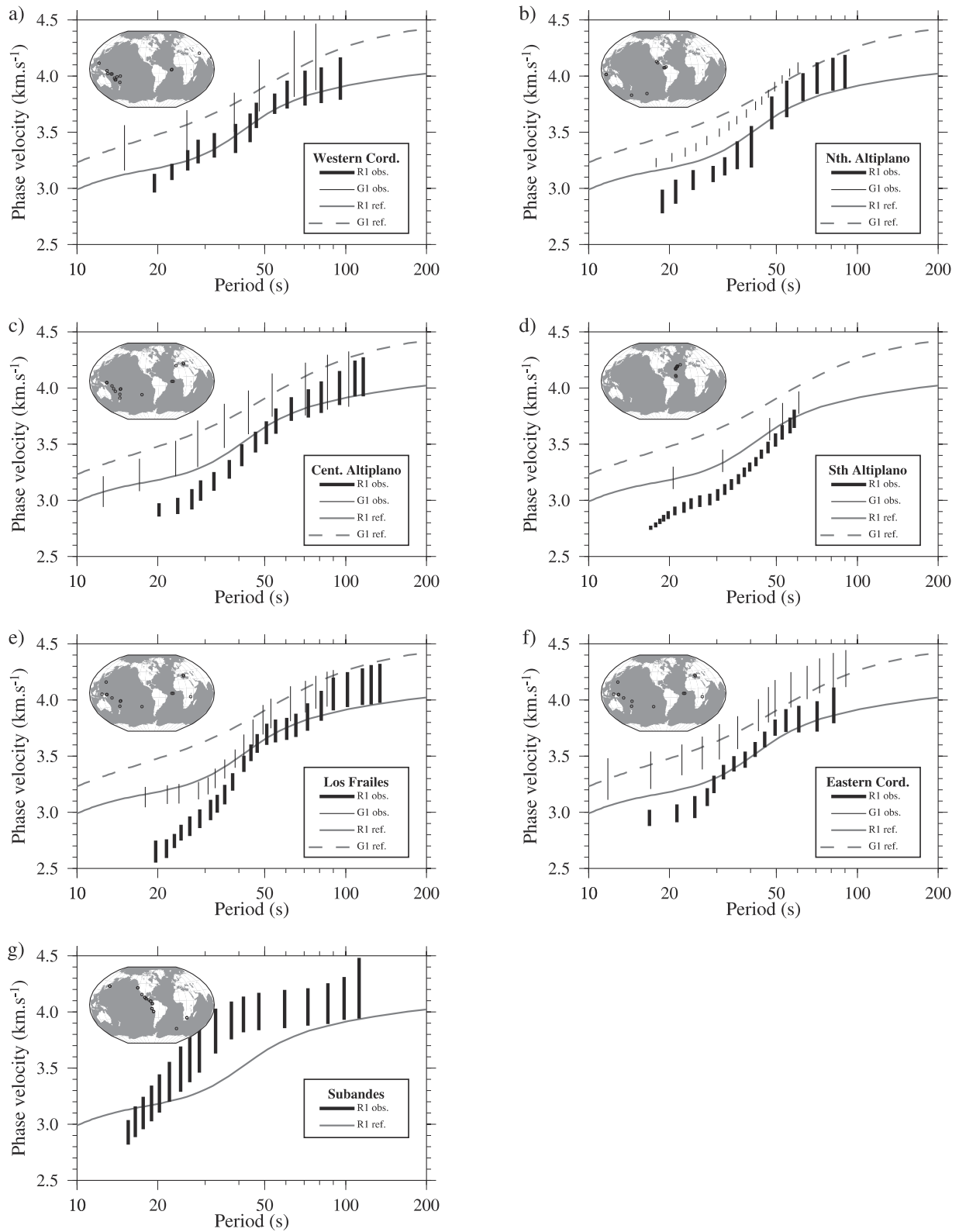


Figure 5. Results of regionalized phase velocity measurements for both Rayleigh (R1) and Love (G1) waves. The solid and dashed lines are the theoretical dispersion curves of the fundamental modes for the reference velocity model presented in Figure 6.

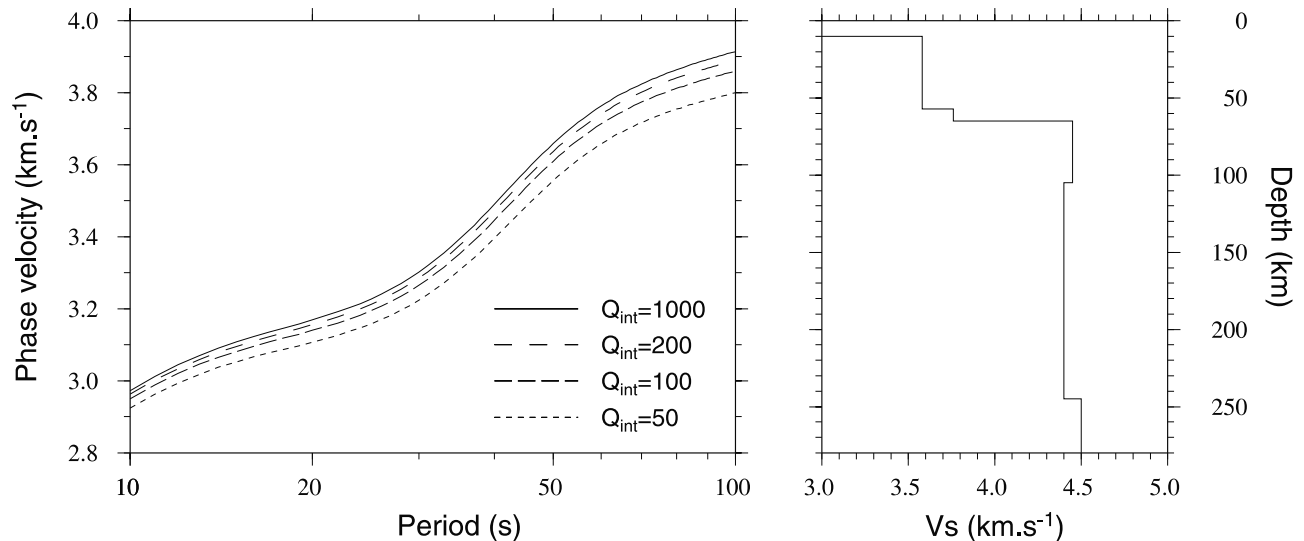


Figure 6. Effect of the anelastic absorption on dispersion curves of the fundamental modes of Rayleigh waves (left) calculated for the reference velocity model (right) with different quality factors. See text for detailed explanations on the velocity model.

respect to a 4.7 km s^{-1} normal upper mantle velocity. We also constrained its depth based on the seismogenic Wadati-Benioff zone [Cahill and Isacks, 1992]. As the sensitivity of phase velocities to velocities in-depth decreases markedly between one-third and half of the wavelength, 1-D models were limited to depths smaller than half the wavelength. Note that none of the constraints listed in Table 1 is very restrictive, and they leave a wide part of the model space open for exploration by the inversion.

4.3. Lithospheric Models

[23] All the V_s models resulting from the inversion are plotted in Figure 7. To make the presentation clearer, the corresponding average 1-D model and its standard deviation computed over a 8-km-thick averaging window were also plotted as black lines. This approach shows that only the long wavelengths of the 1-D model can be resolved using surface wave analysis as one would have expected from the inversion of the fundamental modes only. We checked that these average models are also solutions of the phase velocity inversion. Thus we assumed these average models to be the most representative models among our solutions. In this section, we discuss separately the results obtained for each region and compare them to previously published results.

[24] By receiver function forward modeling, Beck and Zandt [2002] proposed a V_p crustal cross section along the BANJO transect. As the sensitivities of the techniques are different (the receiver functions are sensitive to impedance contrasts whereas the dispersion curves of fundamental modes are mostly sensitive to average V_s), it is worth comparing the results to reduce the existing trade-offs between depth and average velocity. In this study, we will often refer to the results of Beck and Zandt [2002] without restating how they were obtained.

4.3.1. The Western Cordillera

[25] As shown in Figure 7a, the crust of the western Cordillera is fairly normal with an upper crust characterized by a low-to-normal average velocity (3.1 km s^{-1}), and a rather high-velocity lower crust (3.6 km s^{-1}). Note that the

crustal thickness is not constrained by our data but based on Beck *et al.*'s [1996] results. Our average V_s model differs from Beck and Zandt's [2002] in that they found a midcrust LVZ. The existence of such a feature is not precluded by our inversion, but the resolution might be too low to find it. The most striking feature of Figure 7a is a pronounced low-velocity zone (LVZ) in the upper mantle (between ~ 75 and 110 km depth), where V_s may be as low as 4.0 km s^{-1} . At larger depths, we find a high-velocity layer corresponding to the Wadati-Benioff zone even without applying any constraint on the existence of the slab. However, to improve our determination of the velocities within the LVZ, we constrained both the velocity and depth of the slab due to the well established high-velocity slab [Dorbath *et al.*, 1996] at a depth of $100\text{--}120 \text{ km}$ beneath the active volcanic arc.

4.3.2. The Northern Altiplano

[26] Figures 7b, 7c, and 7d show that crustal V_s in the Altiplano are on average lower than the reference model by Zandt *et al.* [1996] (long-dashed line). We do not propose any explanation for these discrepancies because we believe that it would be highly speculative since Zandt *et al.* [1996] proposed a model on P wave velocity, while we inverted for S wave velocity. Moreover, the velocity models strongly vary from north to south within the Altiplano.

[27] The northern Altiplano (Figure 7b) is characterized by a 10-km-thick sedimentary layer with extremely low V_s . Deeper in the midcrust we find a 10-km-thick LVZ, however its thickness is not tightly resolved. The inferred crustal thickness is on average 60 km ($\pm 2 \text{ km}$) that is to say 5 km less than Beck *et al.*'s [1996] estimate. This difference happens because in converting the P_s -to- P time delay to thickness they used a higher crustal average V_s than the one we found. We inferred a rather high upper mantle average V_s in good agreement with the presence of a mantle lid [Whitmann *et al.*, 1992; Myers *et al.*, 1998].

4.3.3. The Central Altiplano

[28] Figure 7c shows that the average velocity within the sedimentary layer of the central Altiplano is higher than in the northern Altiplano (Figure 7b). Between 10 and $\sim 40 \text{ km}$

Table 1. Overview of the Constraints Added to the Inversion of the Dispersion Curves in Each Region^a

Region	L	V_s , km s ⁻¹	T , km	D , km
Western Cordillera	1	$2.74 < V_s < 3.6$	no	$5 < D < 20$
	2	$V_s < 3.8$	$T > 10$	no
	3	$V_s < 4.0$	$T > 10$	no
	4	$V_s < 4.2$	$T > 10$	no
	5	$4.4 < V_s < 4.75$	$T > 20$	$45 < D < 70$
	6	$V_s < 4.8$	$T > 20$	no
	7	$4.8 < V_s < 5.1$	no	$100 < D < 120$
Central Altiplano	1	$2.3 < V_s < 3.2$	no	$7 < D < 12$
	2	$V_s < 3.8$	$T > 10$	no
	3	$V_s < 4.2$	$T > 10$	no
	4	$4.4 < V_s < 4.75$	$T > 20$	$f(\delta P_s - P) \pm 3$
	5	$V_s < 4.8$	$T > 20$	no
	6	$V_s < 4.85$	$T > 20$	no
	7	$4.8 < V_s < 5.1$	no	$160 < D < 180$
Northern Altiplano	1	$2.3 < V_s < 3.2$	no	$7 < D < 12$
	2	$V_s < 3.8$	$T > 10$	no
	3	$V_s < 4.0$	$T > 10$	no
	4	$V_s < 4.2$	$T > 10$	no
	5	$4.4 < V_s < 4.75$	$T > 20$	$f(\delta P_s - P) \pm 3$
	6	$V_s < 4.8$	no	$D < 120$
	7	$4.8 < V_s < 5.1$	no	$5 < T < 15$
Southern Altiplano	1	$2.3 < V_s < 3.5$	no	$5 < T < 15$
	2	$V_s < 3.8$	$T > 10$	no
	3	$V_s < 4.0$	$T > 10$	no
	4	$V_s < 4.2$	$T > 10$	no
	5	$4.4 < V_s < 4.75$	no	$40 < D < 75$
	6	$V_s < 4.8$	$T > 20$	no
	7	$V_s < 4.85$	$T > 20$	no
Los Frailes	1	$2.74 < V_s < 3.6$	$T > 8$	no
	2	$V_s < 3.8$	$T > 10$	no
	3	$V_s < 4.0$	$T > 10$	no
	4	$V_s < 4.2$	$T > 10$	no
	5	$4.4 < V_s < 4.75$	$T > 20$	$55 < D < 70$
	6	$V_s < 4.8$	$T > 20$	no
	7	$V_s < 4.85$	$T > 20$	no
	8	$V_s < 5.1$	no	$D < 200$
Eastern Cordillera	1	$2.74 < V_s < 3.6$	$T > 8$	no
	2	$V_s < 3.8$	$T > 10$	no
	3	$V_s < 4.0$	$T > 10$	no
	4	$V_s < 4.2$	$T > 10$	no
	5	$4.4 < V_s < 4.75$	$T > 20$	$50 < D < 60$
	6	$V_s < 4.8$	$T > 20$	no
	7	$V_s < 4.85$	no	$150 < D$
Sub-Andes	1	$2.74 < V_s < 3.6$	$T > 8$	no
	2	$V_s < 4.0$	no	no
	3	$4.4 < V_s < 4.75$	no	$40 < D < 50$
	4	$V_s < 4.85$	no	$D < 120$

^aThe thickness of a layer (L) is denoted by T and the depth of its upper interface is denoted by D .

depth, our models include a weak V_s gradient in accordance with *Zandt et al.* [1996] and *Swenson et al.*'s [2000] results. Despite the poor resolution of the velocity in the lower crust, there is a general trend toward an increase of velocity with depths. We cannot resolve the thin LVZ found by *Beck and Zandt* [2002] at about 20-km depth beneath the entire plateau at this latitude. The average crustal thickness we infer in this area is the same as in the northern Altiplano.

[29] Above the slab the upper mantle is characterized by a thick LVZ with V_s decreasing to 4.2 km s⁻¹, however, our analysis does not resolve the depth of its upper interface. The local tomography made by *Myers et al.* [1998] shows a high-velocity zone (HVZ) ($V_s = 4.6$ km s⁻¹) underlying the crust which is rather consistent with our results. However, their V_s structure does not exhibit as clearly the LVZ sandwiched in between the high velocities of the mantle lid and slab.

4.3.4. The Southern Altiplano

[30] In the southern Altiplano (Figure 7d), V_s models are very different from those of the central and northern

Altiplano. The first 20 km have a very low average velocity which might be due to a thin LVZ that cannot be resolved. In the midcrust velocities are higher than elsewhere in the Altiplano, whereas at the base of the crust they are lower. We inferred a crustal thickness of about 67 ± 3 km, which is significantly larger than the one of the central Altiplano (60 km). The low velocities at the base of the crust are in good agreement with the observations made by *Schwartz and Kruger* [1997] of a low resistivity zone at a similar depth in the same region. They also agree with the hypothesis proposed by *Wigger et al.* [1994] to explain the lack of energy returning from the lower crust in refraction data collected in this area.

4.3.5. Los Frailes

[31] The Los Frailes ignimbrites are mostly Cenozoic with a few Pleistocene ages measured along its western margin [*de Silva and Francis*, 1991]. The corresponding V_s models are shown in Figure 7e. In the upper crust, they exhibit a 10-km-thick layer with a rather high V_s (3.2 km s⁻¹) underlain by a pronounced 20-km-thick LVZ where the minimal V_s could be as low as 2.6 km s⁻¹. At the base of the crust, our results suggest the existence of a high-velocity zone with average velocities of ~ 4 km s⁻¹. We also find a LVZ in the upper mantle, although its location in-depth remains poorly resolved. Our Los Frailes average model is overall in good accordance with the *Beck and Zandt*'s [2002] crustal model and with the tomographic upper mantle images of *Myers et al.* [1998]. However, the LVZ we identify in the upper mantle is much less pronounced than in *Myers et al.*'s [1998] tomography. Note also that *Baumont et al.* [1999] found in this area a propagation anomaly of the Lg waves which might be due to the presence of the midcrustal LVZ we found in this study.

4.3.6. Eastern Cordillera

[32] Figure 7f shows that we resolved only the gross features of the V_s structure in this area. The crust is characterized by a 25-km-thick layer with a rather constant velocity overlying a lower crust with a strong V_s gradient. We did not resolve second-order features such as the LVZ inferred by *Beck and Zandt* [2002] in the midcrust to lower crust. In the mantle, there is a slight indication of a LVZ at 120 km which is much less pronounced than in the Los Frailes area. However, note that this feature is not seen in the tomographic images of *Myers et al.* [1998], but again, this discrepancy could result from poor resolution.

4.3.7. Sub-Andean Range

[33] Although they are less constrained the dispersion curves obtained in the sub-Andes are very different from those of the other regions (Figure 5), which justifies their inversion for a first-order V_s lithospheric model. This is important because the sub-Andes can therefore be considered as the reference lithospheric structure of the Andes. Figure 7g shows a low V_s upper crust overlying a relatively high V_s lower crust. As already mentioned, the resolution is not good at depth; however, we can see that the upper mantle velocity is higher here than in other regions.

5. Discussion

[34] In this section, we will only discuss the main features of those regional average V_s models that we consider the most robust. Figure 8 shows two east-west and north-south cross sections of the V_s lithospheric structure of the central

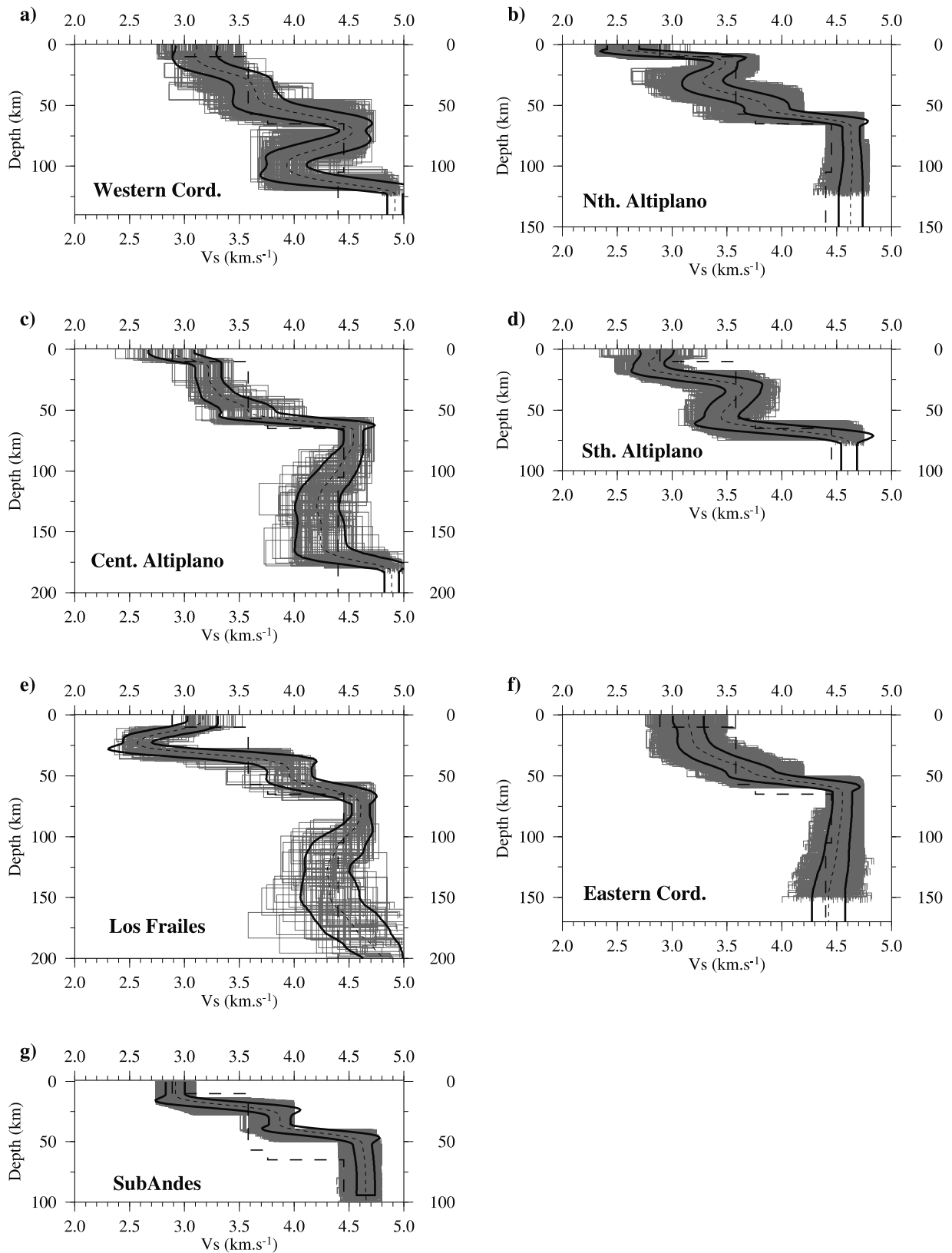


Figure 7. Shear wave velocity models resulting from the inversion of observed phase velocity dispersion curves plotted in Figure 5. In each region, the average model (short dashed line) and its standard deviation (thick black solid line) are superimposed on the solution models (gray solid lines) to highlight the main characteristics of the family of solutions. Note that we checked that the average model is also a solution of the inversion. A reference Andean model based on previous geophysical studies [Zandt *et al.*, 1996; James, 1971] is shown (long dashed line) to easily compare the models obtained in different regions.

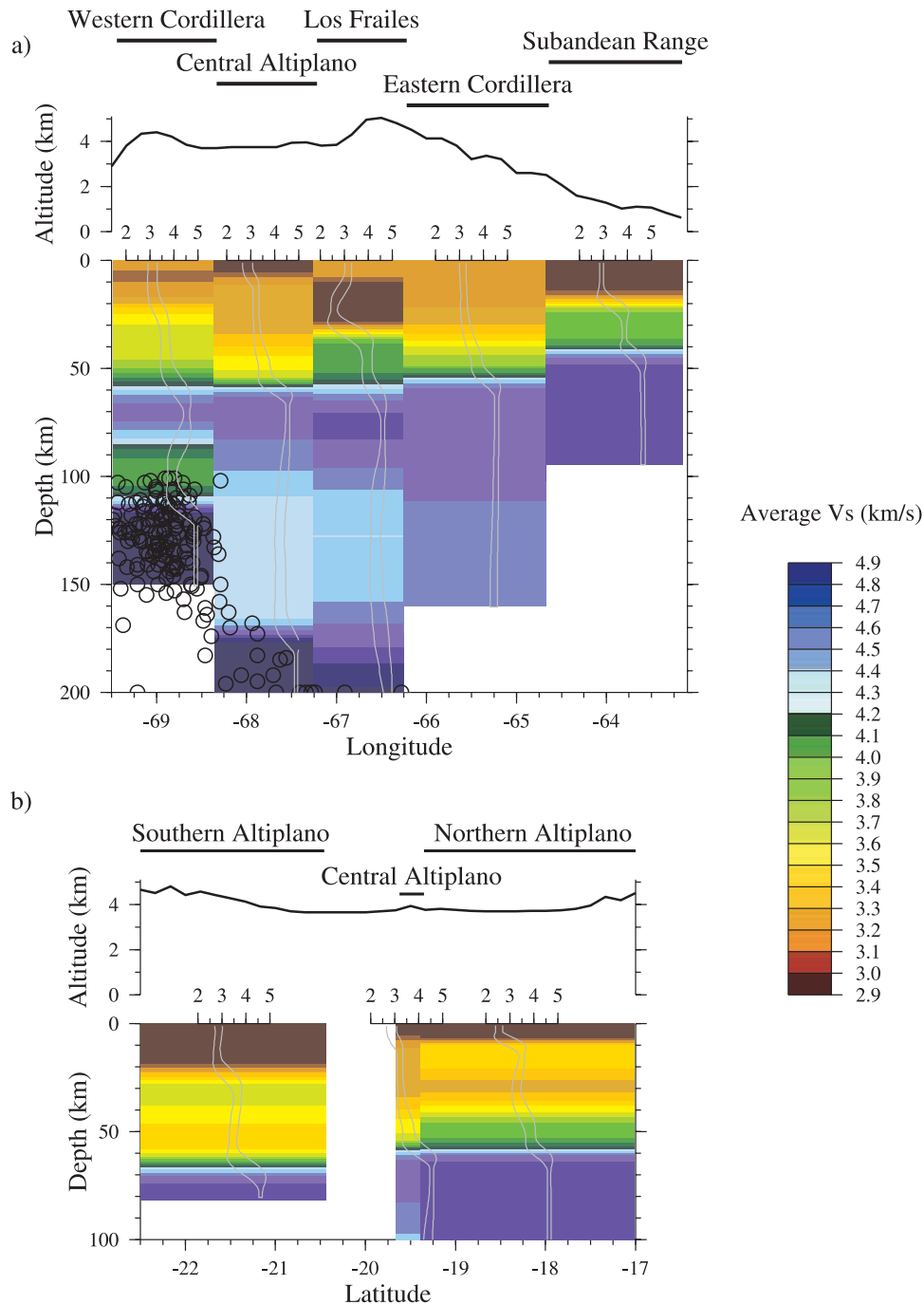


Figure 8. Synthesis of our shear wave velocity estimates on east-west (a) and north-south (b) cross sections. The east-west cross section is located at latitude 20°S and the north-south one is along strike in the Altiplano. In each region, the gray curves delimit the confidence area for the 1-D average V_s model. The color pattern shows the average velocity of each region. See text for detailed explanations. The seismicity of the Wadati-Benioff zone (circles) delineates the location of the slab.

Andes which synthesize our results. Cross sections were obtained by assuming that each region is homogeneous, which is the basic hypothesis of our technique, and that it can be characterized by the estimated average 1-D V_s model shown in Figure 7. The width of each block was determined from the projection of ray paths (plotted in Figure 1) on east-west and north-south profiles.

[35] The most striking feature documented by these cross sections is the tremendous lateral heterogeneity of the V_s

structure both across and along strike of the Andes. At crustal levels, our two main results are the presence of strong low shear wave velocity layers in the upper crust and prominent lateral variations of velocity in the lower crust of the Altiplano.

[36] A strong low V_s layer is found beneath the surface outcrop of the Los Frailes ignimbrites between 10 and 30 km depth (Figure 8a). We interpreted it as the signature of a partially melted zone probably related to the Cenozoic

ignimbritic activity. A similar amplitude low V_s anomaly was inferred in the whole upper crust of the southern Altiplano (Figure 8b). Such a thick anomaly (20 km) cannot be explained only by sediments as the well-known deep sedimentary basins of the northern Altiplano only induce a 10-km-thick, low V_s anomaly. Moreover, the southern part of the corresponding ray paths, known as the Altiplano Puna Volcanic Complex, is one of the largest active ignimbritic fields [de Silva, 1989; de Silva et al., 1994] whose crust includes a very thin (1 km), extremely low V_s (<0.5 km s⁻¹) layer located at ~ 20 km depth [Chmielowski et al., 1999]. We believe that this is a second explanation for our 20-km-thick low V_s anomaly in the southern Altiplano. A similar anomaly is visible in the sub-Andean Range in Figure 8a. However, since the depth of its lower boundary is questionable due to poor resolution, the anomaly can be fully interpreted as due to sediments.

[37] At lower crustal levels, Figure 8a displays a striking contrast between the central Altiplano, which has low velocities, and the other regions. This result of a low V_s lower crust in the Altiplano compares well to the similar observations made for V_p in this region [Zandt et al., 1996; Swenson et al., 1999; Beck and Zandt, 2002] that were considered to be due to a predominantly felsic crustal composition in a medium with a high geotherm, nearly but not quite reaching melting conditions. The higher V_s we find in the surrounding regions suggests that the lower crust could have an intermediate to mafic composition.

[38] Along-strike variations of the crustal V_s structure in the Altiplano are as spectacular as across-strike. Figure 8b shows that the transition from the Altiplano to the Puna is characterized by a crustal thickening from ~ 60 to 67 km, in correlation with an increase in elevations, which are on average 1 km higher in the Puna. Another along-strike difference is that the lower crust of the southern Altiplano has the lowest velocities estimated at these depths in the whole area. We already discussed the comparison of these results with those previously obtained by magnetotelluric and refraction studies.

[39] At mantle levels, the subducted Nazca plate (depicted by the seismicity), is overlaid by an eastward dipping LVZ that weakens downward. We interpret this feature as the signature of an elongated magma generation zone caused by the release of hydrated materials buried with the slab. The strength of the V_s anomaly probably reflects differences in partial melting rate. In the sub-Andean Range, the mantle S wave velocities are higher on average than in the other regions and may reflect the presence of the cold and thick lithosphere of the Brazilian shield. Note that there is an indication for the thinning of the lithosphere toward the west in the continuous rise of the 4.5 km s⁻¹ velocity contour from the eastern to the western Cordilleras. However, our observations do not provide a firm answer to the question of the fate of the subducting Brazilian shield below the Andes.

6. Conclusion

[40] Regionalized surface wave dispersion curves were measured from all the available broadband teleseismic records in the central Andes and inverted for 1-D V_s models. Our results show strong lateral variations of the V_s structure in good correlation with the morphotectonic units defined

from geologic studies. Prominent low-velocity anomalies probably related to partial melt are found in the upper crust beneath the Los Frailes ignimbrite complex and the southern Altiplano. At lower crustal level, the Altiplano is characterized by lower V_s than the surrounding regions revealing differences in composition. In the transition zone between the Altiplano and the Puna, we find that the crust thickens in correlation with an increase in elevations. In the mantle, the Nazca plate is found to be overlaid by a dipping low velocity zone with decreasing intensity with depth. Such a feature is interpreted as a magma generation zone. The rather high velocities found in the upper mantle just below the crust favor the idea of a cold mantle lid underlying the whole central Andes. Since V_s is more sensitive to temperature and fluid content than V_p , we have shown that this technique efficiently complements previous geophysical investigations. The next step is the joint inversion of receiver functions and dispersion curves.

[41] **Acknowledgments.** Funding for the BANJO experiment was provided by NSF grants EAR-9304949, EAR-9614250, and EAR-9304560 at the University of Arizona and Carnegie Institution of Washington, respectively. The APVC experiment was funded by NSF grant EAR-9505816 at the University of Arizona. The SEDA experiment was funded by the IGPP program at Lawrence Livermore National Laboratory. This work has been also supported by ATP Tomographie 1996 of INSU/CNRS. We would like to thank all the members of the field crews. We are very thankful to Nicolas Shapiro for providing us his semiglobal inversion code. Most of the calculations were performed at the Centre de Calcul Intensif de l'Observatoire de Grenoble. We are grateful to the reviewers of the paper for their remarks helping us to improve this study and Valerie Maupin for her contribution to the final version.

References

- Aki, K., and P. G. Richards, *Quantitative Seismology Theory and Methods*, edited by A. Cox, W. H. Freeman, New York, 1980.
- Azimi, S. A., A. V. Kalinin, V. V. Kalinin, and B. L. Pivovarov, Impulse and transient characteristics of media with linear and quadratic absorption laws, *Izv. Phys. Solid Earth*, 2, 88–93, 1968.
- Baumont, D., A. Paul, S. Beck, and G. Zandt, Strong crustal heterogeneity in the Bolivian Altiplano as suggested by attenuation of Lg waves, *J. Geophys. Res.*, 104, 20,287–20,305, 1999.
- Beck, S., and G. Zandt, The nature of orogenic crust in the central Andes, *J. Geophys. Res.*, 107(B10), 2230, doi:10.1029/2000JB000124, 2002.
- Beck, S. L., G. Zandt, S. C. Myers, T. C. Wallace, P. G. Silver, and L. Drake, Crustal-thickness variations in the central Andes, *Geology*, 24, 407–410, 1996.
- Brune, J., and J. Dorman, Seismic waves and earth structure in the Canadian shield, *Bull. Seismol. Soc. Am.*, 53, 167–210, 1963.
- Cahill, T. A., and B. L. Isacks, Seismicity and shape of the subducted Nazca plate, *J. Geophys. Res.*, 97, 17,503–17,529, 1992.
- Chmielowski, J., G. Zandt, and C. Haberland, The central Andean Altiplano-Puna magma body, *Geophys. Res. Lett.*, 26, 783–786, 1999.
- Cotte, N., H. A. Pedersen, M. Campillo, V. Farra, and Y. Cansi, Off-great circle propagation of intermediate period surface waves as observed on a dense array in the French Alps, *Geophys. J. Int.*, 142, 825–840, 2000.
- de Silva, S. L., Altiplano-Puna volcanic complex of the central Andes, *Geology*, 17, 1102–1106, 1989.
- de Silva, S. L., and P. W. Francis, *Volcanoes of the central Andes*, Springer-Verlag, New York, 1991.
- de Silva, S. L., S. Self, P. W. Francis, R. E. Drake, and R. R. Carlos, Effusive silicic volcanism in the central Andes: The Chao dacite and other young lavas of the Altiplano-Puna volcanic complex, *J. Geophys. Res.*, 99, 17,805–17,825, 1994.
- Dorbath, C., and F. Masson, Composition of the crust and upper-mantle in the central Andes (19°30'S) inferred from P wave velocity and Poisson's ratio, *Tectonophysics*, 327, 213–223, 2000.
- Dorbath, C., and A. Paul, Tomography of the Andean crust and mantle at 20°S: First results of the Lithoscope experiment, *Phys. Earth Planet. Inter.*, 97, 133–144, 1996.
- Dorbath, C., M. Granet, G. Poupinet, and C. Martinez, A teleseismic study of the Altiplano and the Eastern Cordillera in Northern Bolivia: New constraints on a lithospheric model, *J. Geophys. Res.*, 98, 9825–9844, 1993.

- Dziewonski, A., S. Bloch, and N. Landisman, A technique for the analysis of transient seismic signals, *Bull. Seismol. Soc. Am.*, 59, 427–444, 1969.
- Eaton, G. P., Geophysical and geological characteristics of the crust of the Basin and Range province, in *Continental Tectonics*, pp. 96–113, Natl. Acad. of Sci., Washington, D. C., 1980.
- Gumper, F., and P. W. Pomeroy, Seismic wave velocities and earth structure on the African continent, *Bull. Seismol. Soc. Am.*, 60, 651–668, 1970.
- Herrmann, R. B., Some aspects of band-pass filtering of surface waves, *Bull. Seismol. Soc. Am.*, 63, 663–671, 1973.
- Herrmann, R. B., *Computer Programs in Seismology*, vol. IV, *Surface Waves Inversion*, Saint Louis Univ., St. Louis, Mo., 1987.
- Huestis, S., P. Molnar, and J. Oliver, Regional Sn velocities and shear velocity in the upper mantle, *Bull. Seismol. Soc. Am.*, 63, 469–475, 1973.
- James, D. E., Andean crustal and upper mantle structure, *J. Geophys. Res.*, 76, 3246–3271, 1971.
- Laske, G., and G. Masters, Surface wave polarization data and global anisotropic structure, *Geophys. J. Int.*, 132, 508–520, 1998.
- Laske, G., G. Masters, and W. Zurn, Frequency-dependent polarization measurements of long-period surface waves and their implications for global phase-velocity maps, *Phys. Earth Planet. Inter.*, 84, 111–137, 1994.
- Levshin, A. L., T. B. Yanovskaya, A. V. Lander, B. G. Bukchin, M. P. Barmin, L. I. Ratnikova, and E. N. Its, Recording, identification, and measurement of surface wave parameters, in *Seismic Surface Waves in a Laterally Inhomogeneous Earth*, edited by V. I. Keilis-Borok, pp. 131–182, Kluwer Acad., Norwell, Mass., 1989.
- Liu, H. P., D. L. Anderson, and H. Kanamori, Velocity dispersion due to an elasticity: Implications for seismology and mantle composition, *Geophys. J. R. Astron. Soc.*, 47, 41–58, 1976.
- Masson, F., C. Dorbath, C. Martinez, and G. Carlier, Local earthquake tomography of the Andes at 20°S: Implication for the structure and building of the mountain range, *J. S. Am. Earth. Sci.*, 13, 3–19, 2000.
- McGarr, A., Amplitude variations of rayleigh waves-horizontal refraction, *Bull. Seismol. Soc. Am.*, 59, 1307–1334, 1969.
- Myers, C. M., S. Beck, G. Zandt, and T. Wallace, Lithospheric-scale structure across the Bolivian Andes from tomographic images of velocity and attenuation for P and S waves, *J. Geophys. Res.*, 103, 21,233–21,252, 1998.
- Ni, J., and M. Barazangi, High-frequency seismic wave propagation beneath the Indian Shield, Himalayan arc, Tibetan plateau and surrounding regions: High uppermost mantle velocities and efficient Sn propagation beneath Tibet, *Geophys. J. R. Soc.*, 72, 665–689, 1983.
- Ocola, L. C., and R. P. Meyer, Crustal low-velocity zones under the Peru-Bolivian Altiplano, *Geophys. J. R. Astron. Soc.*, 30, 199–209, 1972.
- Oliver, J., A summary of observed seismic surface wave dispersion, *Bull. Seismol. Soc. Am.*, 52, 81–86, 1962.
- Schmitz, M., W.-D. Heisohn, and F. R. Schilling, Seismic, gravity and petrological evidence for partial melt beneath the thickened central Andean crust (21–23°S), *Tectonophysics*, 270, 313–326, 1997.
- Schwartz, G., and D. Krüger, Resistivity cross section through the southern central Andes as inferred from magnetotelluric and geomagnetic deep soundings, *J. Geophys. Res.*, 102, 11,957–11,978, 1997.
- Schwartz, G., G. Chong Dias, D. Kruger, E. Martinez, W. Massow, V. Rath, and J. G. Viramonte, Crustal high conductivity zones in the southern central Andes, in *Tectonics of the Southern Central Andes*, edited by K.-J. Reutter, E. Scheuber, and P. J. Wigger, pp. 49–67, Springer-Verlag, New York, 1994.
- Shapiro, N. M., M. Campillo, A. Paul, S. K. Singh, D. Jongmans, and F. J. Sanchez-Sesma, Surface-wave propagation across the Mexican volcanic belt and the origin of the long-period seismic wave amplification in the valley of Mexico, *Geophys. J. Int.*, 128, 151–166, 1997.
- Swenson, J., S. Beck, and G. Zandt, Regional distance shear-coupled P-waves within the northern Altiplano, *Geophys. J. Int.*, 139, 743–755, 1999.
- Swenson, J., S. L. Beck, and G. Zandt, Crustal structure of the Altiplano from broadband regional waveform modeling: Implications for the composition of thick continental crust, *J. Geophys. Res.*, 105, 607–621, 2000.
- Taylor, S. R., and M. N. Toksoz, Measurement of interstation phase and group velocities and Q using Wiener filtering, *Bull. Seismol. Soc. Am.*, 72, 73–91, 1982.
- Whitmann, D., B. L. Isacks, J.-L. Chatelain, J.-M. Chiu, and A. Perez, Attenuation of high frequency seismic waves beneath the central Andean plateau, *J. Geophys. Res.*, 97, 19,929–19,947, 1992.
- Wigger, P., M. Schmitz, M. Areneda, G. Asch, S. Baldzuhn, P. Giese, W.-D. Heisohn, E. Martinez, E. Ricaldi, P. Rower, and P. Viramonte, Variation in the crustal structure of the southern central Andes deduced from seismic refraction investigations, in *Tectonics of the Southern Central Andes*, edited by K.-J. Reutter, E. Scheuber, and P. J. Wiggers, pp. 23–48, Springer-Verlag, New York, 1994.
- Zandt, G., A. A. Velasco, and S. L. Beck, Composition and thickness of the southern Altiplano crust, Bolivia, *Geology*, 22, 1003–1006, 1994.
- Zandt, G., S. L. Beck, S. R. Ruppert, C. J. Ammon, D. Rock, E. Minaya, T. C. Wallace, and P. G. Silver, Anomalous crust of the Bolivian Altiplano, central Andes: Constraints from broadband regional seismic waveforms, *Geophys. Res. Lett.*, 23, 1159–1162, 1996.

D. Baumont, IRSN/DPRE/SERGD/BERSSIN, BP17, 92262 Fontenay-aux-Roses, France. (david.baumont@irsn.fr)

S. Beck, and G. Zandt, Southern Arizona Seismological Observatory and Department of Geosciences, University of Arizona, Tucson, AZ 85721, USA. (beck@geo.arizona.edu; zandt@geo.arizona.edu)

A. Paul, and H. Pedersen, Laboratoire de Géophysique Interne et Tectonophysique, BP 53, F-38041 Grenoble, Cedex 9, France. (apaul@lgit.obs.ujf-grenoble.fr; pedersen@lgit.obs.ujf-grenoble.fr)